Journal of Nuclear Materials 424 (2012) 171–175

Contents lists available at SciVerse ScienceDirect

Journal of Nuclear Materials

journal homepage: www.elsevier.com/locate/jnucmat

Letter to the Editor

Microwave synthesis and properties of fine-grained oxides dispersion strengthened tungsten

R. Liu, Y. Zhou, T. Hao, T. Zhang, X.P. Wang, C.S. Liu, Q.F. Fang *

Key Laboratory of Materials Physics, Institute of Solid State Physics, Chinese Academy of Sciences, Hefei 230031, China

ARTICLE INFO

Article history:
Received 27 December 2011
Accepted 2 March 2012
Available online 10 March 2012

ABSTRACT

Dense W, W–1 wt%La_2O_3 and W–1 wt%Y_2O_3 samples with fine microstructure were fabricated by microwave sintering method using nano-scaled powders. The FESEM and TEM analysis, thermal conductivity and Vickers micro-hardness measurements were exploited to characterize these samples. It is found that the addition of Y_2O_3 and La_2O_3 nano-particles could significantly hinder the grain growth of tungsten in the consolidation process, decreasing the average grain size from 3.2 μm in pure W down to 0.7 μm in W–1%Y_2O_3 sample. The thermal conductivity and relative density of these samples are higher than 120 W/m K and in the range of 95–97%, respectively. The Vickers hardness of W–1%Y_2O_3 sample reaches as high as 6.91 GPa, 30% higher than that of pure W (5.04 GPa).

1. Introduction

Tungsten is considered as one of the most promising candidates for plasma facing materials in fusion reactors (ITER and the future DEMO reactor) and for spallation neutron source target applications due to its high melting point, high sputtering resistance, low tritium retention, and low thermal expansion [1–5]. However, tungsten exhibits severe embrittlement in several aspects, including low-temperature brittleness, recrystallization brittleness and radiation induced brittleness [5–7]. Nanotechnology provides a possible access to high performance tungsten based materials. It was reported that ultrafine-grained tungsten produced by severely plastic deformation shows reduced brittleness and improved toughness [7–9]. Besides, the large amount of grain boundaries in nano-grained and ultrafine-grained materials can serve as effective sinks for irradiation induced point defects, and thus increases the resistance to irradiation damage of the materials [7,10–12]. Nevertheless, the high temperature and long holding time necessary for the consolidation of tungsten powders will result in significant grain growth. Therefore, the mechanical properties and irradiation resistance of nano-structured tungsten ever prepared would be degraded with the grain coarsening that may occur at working temperature.

Recently, nano-structured but thermally stable oxide dispersion strengthened tungsten materials have attracted intense interest. The dispersion of small amounts of oxide nano-particles, such as ThO_2, La_2O_3, Y_2O_3, HfO_2, and CeO_2, in the so-called oxide dispersion strengthened tungsten (ODS-W), could inhibit the grain growth during the sintering process and stabilize the microstructure when exposed to high temperature [13–18]. Besides, the dispersed oxides could increase high temperature strength, creep resistance, and the recrystallization temperature of tungsten [18–20]. Furthermore, the addition of Y_2O_3 could even increase the oxidation resistance of tungsten [20,21]. However, the sintering of nano-sized powders into dense bulk metal with nano-structure remains to be a challenge. Conventional sintering of tungsten is commonly carried out at temperatures as high as 2000–2500 °C for a long sintering time [19]. When exposed to such high sintering temperature for long time, tungsten nano-particles usually grow rapidly to reduce the high surface energy despite the restriction of grain movement by oxide particles [13,15]. Therefore, to obtain fine-grained tungsten materials, it is essential to reduce the sintering temperature and time. Among various novel sintering techniques, spark plasma sintering (SPS), hot isostatic pressing (HIP) and microwave sintering were often used for the fabrication of fine-grained materials. SPS method is widely used to synthesize refractory metals and their carbides, due to its fast heating and short holding time [13,19,22]. HIP is another effective method for fabricating ultrafine grained tungsten with high density owing to the high pressure in the sintering process [6,7]. Microwave sintering has been frequently utilized in the consolidation of ceramics and powdered metals including refractory metals and their carbides [23–27]. In the microwave sintering process, the powdered samples absorb microwave energy and heat themselves from the very interior. Therefore, microwave sintering possesses also advantages of rapid heating rate and short sintering time [23,25], which are beneficial to inhibiting the grain growth.

In the present work, dense fine-grained ODS tungsten samples were fabricated with microwave sintering method from the

* Corresponding author. Tel.: +86 551 5591459; fax: +86 551 5591434.
E-mail address: qffang@issp.ac.cn (Q.F. Fang).

0022-3115/$ - see front matter © 2012 Elsevier B.V. All rights reserved.
http://dx.doi.org/10.1016/j.jnucmat.2012.03.008

nano-sized tungsten powders, La_2O_3 and Y_2O_3 nano-particles. The effects of La_2O_3 and Y_2O_3 nano-particles addition on the consolidation behavior, microstructure, hardness and thermal conductivity of ODS tungsten samples were investigated by comparing to the pure tungsten samples.

2. Experimental details

Pure tungsten samples and ODS-W samples with compositions of W–1 wt%La_2O_3 and W–1 wt%Y_2O_3 were synthesized. Pure W (particle size 20–100 nm and purity >99.9%), La_2O_3 (particle size 10–50 nm, purity >99.99%) and Y_2O_3 (particle size 10–50 nm, purity >99.99%) powders were used as the starting materials. Powders were milled in a planetary ball mill for 4 h. Agate balls and agate mortars were used. A ball-to-powder weight ratio of 8:1 and a rotation speed of 240 rpm were adopted. The ball-milled powders were heated at 780 °C for 1 h and cooled down to room temperature in a flowing H_2 atmosphere. Then the powders were pressed into a cylinder mold at 400 MPa in air without any binders. The cylindrical green compacts are 13 mm in diameter and about 3 mm in height.

Microwave sintering was carried out in a multimode microwave furnace (HAMiLab-V3000, Changsha Syno-therm Co., Ltd., China) with a 0.3–3 kW microwave generator operated at 2.45 GHz. Temperature was monitored by an infrared pyrometer (Raytek RAYMM2MHSF1L) installed at the top of the vacuum chamber. The sintering conditions were described in detail elsewhere [29,30]. The temperature profile of the sintering program was illustrated in Fig. 1. All samples in this study were microwave-sintered following the same sintering program.

The density of sintered samples was determined by Archimedes' principle. The theoretical density of the ODS-W composites was calculated from the fraction and theoretical density of each component. The theoretical density of tungsten, La_2O_3 and Y_2O_3 was adopted as 19.3, 6.51 and 5.01 g/cm^3, respectively. Polished samples were subjected to Vickers micro-hardness measurement at room temperature with a load of 100 g and a dwell time of 10 s. Thermal diffusivity (α) was measured by the laser flash diffusivity system (LFA457 Micro flash, NETZSCH). The thermal conductivity (λ) was calculated from the thermal diffusivity (α), density (ρ) and specific heat (C_p) according to the relation $\lambda = \alpha C_p \rho$. The specific heat data was adopted from Ref. [28]. Microstructure of specimens was characterized with a field-emission scanning electron microscopy (FESEM, Sirion 200, FEI) and a transmission electron microscope (TEM, JEM-2000FX). Energy dispersive X-ray (EDX, INCA) analytical system installed on TEM was used for elemental analysis.

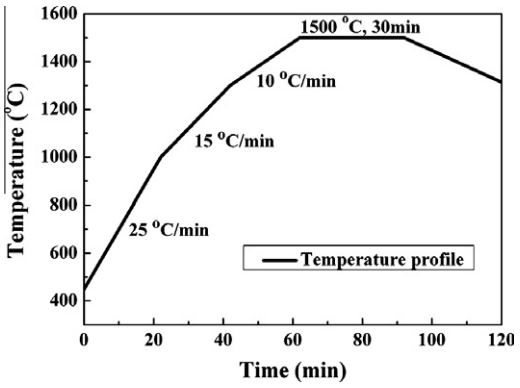

Fig. 1. Temperature profile for the sintering of the pure tungsten and ODS-W materials.

3. Results and discussion

The SEM micrographs of as-received and ball-milled tungsten powders are plotted in Fig. 2. As shown in Fig. 2a, the as-received tungsten powders are spherical with an average particle size of 20–100 nm and exhibit severe aggregation. After ball-milling, the powders are less aggregated and become a little plate-like, as shown in Fig. 2b.

Density of the microwave consolidated samples was listed in Table 1. It can be seen that the density of pure tungsten is about 18.7 g/cm^3, corresponding to a relative density of 96.9%. The relative density of the W–1%Y_2O_3 sample is about 96.8%. However, the relative density of the W–1%La_2O_3 sample sintered at the same condition is only about 95%. This indicates that the W–1%Y_2O_3 sample exhibits better sinterability than the W–1%La_2O_3 sample. Kim et al. [13] have also found that the W–Y_2O_3 system exhibits the highest sinterability among the W–Y_2O_3, W–HfO_2, and W–La_2O_3 systems when they were consolidated by SPS method. They suggested that liquid-like phases composed of W, Y and O were formed during sintering process, which facilitated the consolidation of the W particles.

The relative density of about 97% for the microwave-sintered pure tungsten and W–1%Y_2O_3 samples is relatively high if one notices that the sintering temperature is only 1500 °C and the holding time is just 30 min. In comparison, for the pure tungsten and W–Y_2O_3 samples sintered by conventional method at 2200 °C for 1 h the relative density is lower than 95% [19]. For the W–1%Y_2O_3 sample sintered by SPS the relative density can reach 97%, but the sintering temperature is as high as 1700 °C [13].

The surface and cross section of pure W was directly characterized by SEM without polishing or etching. Fig. 3a reveals the nearly fully dense surface of microwave-sintered tungsten, in agreement with the high relative density of 97%. The grain size of tungsten

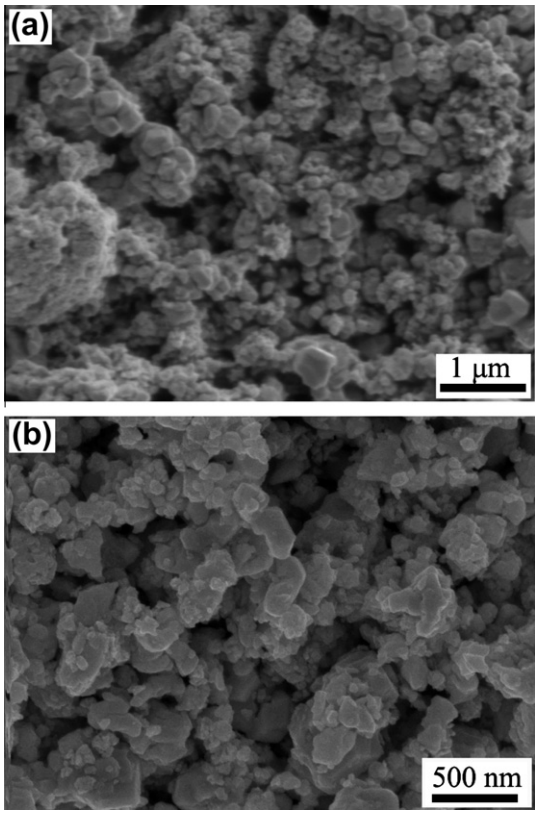

Fig. 2. SEM images of: (a) as-received W powders and (b) the ball-milled W nanopowders.

Table 1
Density, grain size, Vickers micro-hardness and thermal conductivity of pure W and ODS-W samples microwave-sintered at 1500 °C for 30 min.

Materials	Density (g/cm^3)	Relative density (%)	Grain size (μm)	H_{V100g} (GPa)	Thermal conductivity W/(m K)
W	18.7	96.9 ± 0.3	3.2	5.04 ± 0.25	156
W–1 wt%La_2O_3	18.0	95.0 ± 0.3	1.4	4.21 ± 0.25	121
W–1 wt%Y_2O_3	18.2	96.8 ± 0.3	0.7	6.91 ± 0.20	131

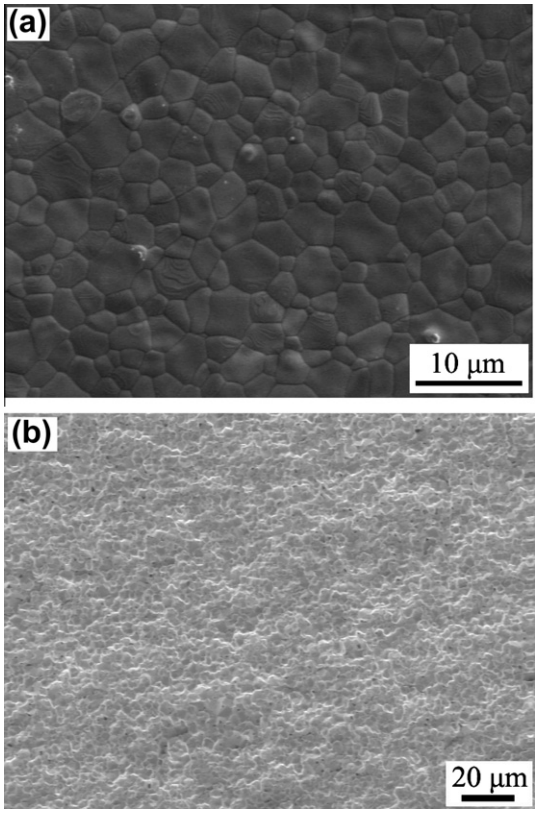

Fig. 3. Micrographs of pure tungsten microwave-sintered at 1500 °C for 30 min: (a) surface and (b) fracture surface.

is in the range of 1–6 μm, which is much larger than that of initial powders (Fig. 2a and b), indicating obvious grain growth in pure tungsten owing to the high surface energy of the nano-sized tungsten particles. Fig. 3b shows the fracture surface of pure tungsten at a relative low magnification. Uniform microstructure with very low level of porosity was revealed.

The fracture surfaces of W–1%La_2O_3 and W–1%Y_2O_3 samples were presented in Fig. 4b and c, where the results of pure tungsten at the same magnification was shown for comparison (Fig. 4a). The fresh fracture surface was obtained by breaking the specimens at room temperature. Pure tungsten and W–1%Y_2O_3 exhibited lower porosity as compared to W–1%La_2O_3. More careful analysis of Fig. 4 revealed that the fracture surface is typical intergranular, indicating that these samples are all brittle at room temperature.

From Fig. 4 it can be clearly seen that La_2O_3 and Y_2O_3 nano-particles have a significant grain refinement effect on tungsten. Pure tungsten exhibits coarse grain size, as shown in Fig. 4a. The W–1%Y_2O_3 exhibits the smallest grain size (Fig. 4c) as compared to pure tungsten (Fig. 4a) and W–1%La_2O_3 (Fig. 4b).

The grain size distribution was determined from the SEM micrographs for pure W, W–1%La_2O_3 and W–1%Y_2O_3 samples and shown in Fig. 5. The grain size distribution of pure tungsten is wide, in the range from 0.5 to 7.5 μm with an average value of 3.2 μm, while those of W–1%La_2O_3 and W–1%Y_2O_3 are relatively narrow, in the range from 0.3 to 3.9 μm, and from 0.2 to 1.6 μm,

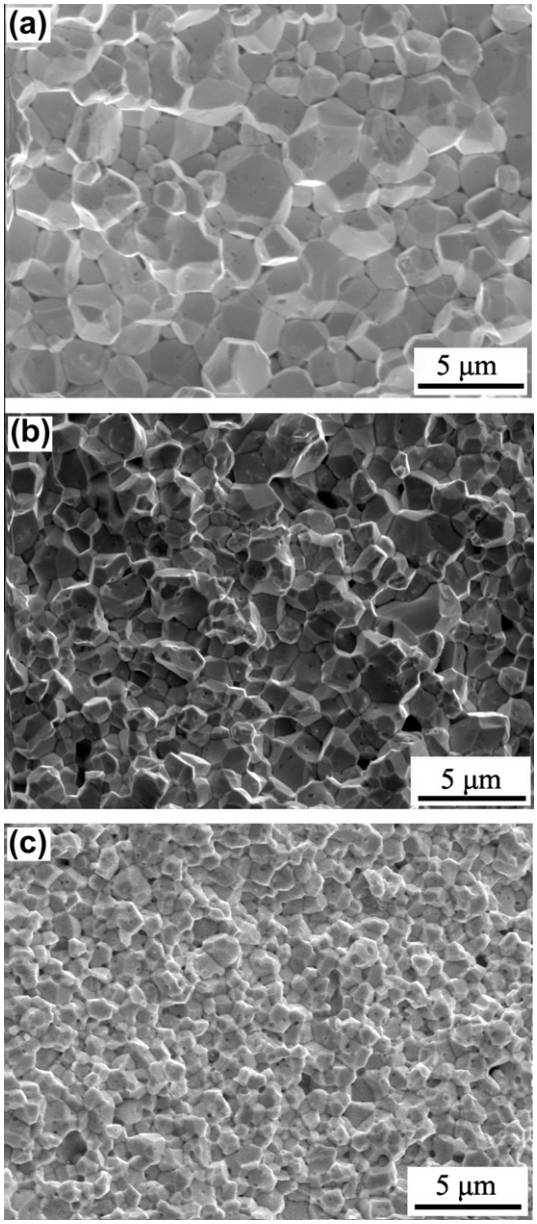

Fig. 4. SEM micrographs of fracture surface for: (a) pure W, (b) W–1%La_2O_3, and (c) W–1%Y_2O_3 microwave-sintered at 1500 °C.

respectively. The average grain size of sintered W–1%La_2O_3 and W–1%Y_2O_3 is about 1.4 and 0.7 μm, respectively, which are much smaller than that of pure tungsten, as listed in Table 1. These results demonstrate that oxide nano-particles such as La_2O_3 and Y_2O_3 are effective in hindering the grain growth of tungsten in the sintering process, and Y_2O_3 is more prominent than La_2O_3 in the grain refinement of tungsten.

Yar et al. [15,17] fabricated W–Y_2O_3 and W–La_2O_3 samples by SPS method from chemically synthesized nano-powders. They

reported an average grain size of about 2.3 and 4.2 μm for the W–1%Y_2O_3 samples sintered at 1200 °C and the W–0.9%La_2O_3 samples sintered at 1300 °C, respectively. In the present work however, much smaller grain size (0.7 and 1.4 μm) were obtained for W–1%Y_2O_3 and W–1%La_2O_3 samples even though they were microwave-sintered at 1500 °C.

The TEM characterization of a W–1%Y_2O_3 sample was presented in Fig. 6. It can be seen that most of the nano-sized oxide particles are dispersed on the grain boundary of tungsten and the size of oxide particles is around 50 nm (Fig. 6a). Therefore, it is clear that the nano-sized oxide particles on the grain boundaries significantly hinder the grain growth of tungsten during the microwave sintering process and result in the formation of fine-grained W–1%Y_2O_3 samples. As shown in Fig. 7, the EDX analysis from the oxide phases in W–1%Y_2O_3 samples revealed that the phase is made up of only W, Y and O with an approximate atomic ratio of 15:13:72, which is in agreement with the suggestion of Kim et al. [13].

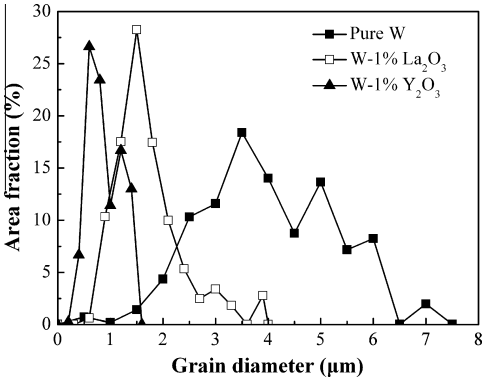

Fig. 5. Grain size distribution of pure W, W–1%La_2O_3 and W–1%Y_2O_3 samples.

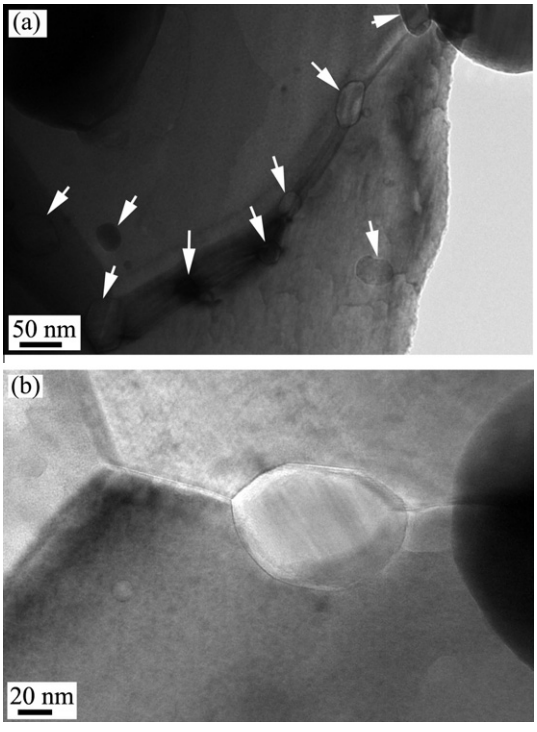

Fig. 6. TEM micrographs of dispersed particles in W–1%Y_2O_3: (a) overview of tungsten grains and oxide particles and (b) detail of oxide particle on the grain boundary of tungsten.

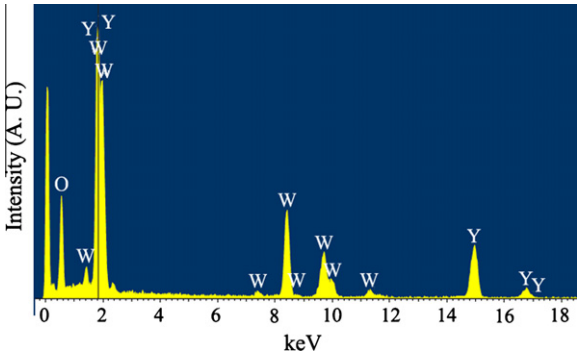

Fig. 7. EDX spectra of the oxide phase in W–1%Y_2O_3 microwave-sintered at 1500 °C for 30 min.

Vickers micro-hardness of pure W, W–1%La_2O_3 and W–1%Y_2O_3 samples are about 5.04, 4.21, and 6.91 GPa, respectively, as listed in Table 1. Of all the three kinds of tungsten materials, the W–1%Y_2O_3 sample exhibits highest hardness, which is 30% higher than that of pure tungsten sample. However, in the case of La_2O_3 dispersed tungsten sample, the hardness is much lower than that of pure tungsten sample. The low hardness of W–1%La_2O_3 sample may originate from the lower relative density even though La_2O_3 dispersed tungsten sample has smaller grain size than the pure tungsten sample.

The thermal conductivity at room temperature of pure W, W–1%La_2O_3 and W–1%Y_2O_3 samples are 156, 131, 121 W/m K, respectively, as listed in Table 1. The thermal conductivity of microwave-sintered pure W sample is close to the literature data of pure W (about 160 W/m K at room temperature [31]), while those of W–1%La_2O_3 and W–1%Y_2O_3 samples are a little lower. This may be originated from the low relative density, the large amount of grain boundaries due to the small grain size, and the addition of low thermally conductive oxides in ODS-W samples. However, it is worth noting that the thermal conductivity of all samples is above 120 W/m K.

4. Conclusions

Dense pure tungsten, W–1%La_2O_3 and W–1%Y_2O_3 samples were microwave-sintered at 1500 °C for 30 min from nano-scaled powders. The relative density of pure tungsten and W–1%Y_2O_3 samples is near 97%, higher than that of W–1%La_2O_3 (95%). The dispersion of La_2O_3 and Y_2O_3 nano-particles could significantly inhibit the grain growth of tungsten during consolidation, and Y_2O_3 has better effect on the grain refinement than La_2O_3. Besides, W–1%Y_2O_3 sample has a higher hardness than pure tungsten and W–1%La_2O_3 samples. However, ODS-W samples show lower thermal conductivity than pure tungsten. The toughness and thermal-shock tests remain to be completed in further work. In summary, Y_2O_3 addition in tungsten is more effective in densifying, strengthening and grain refining than La_2O_3 addition, and microwave sintering method is an effective technique for fabricating dense tungsten with fine microstructure.

Acknowledgements

This work was financially supported by the Innovation Program (Grant No. KJCX2-YW-N35) and Strategic Priority Research Program (Grant No. XDA03010303) of Chinese Academy of Sciences, by the National Magnetic Confinement Fusion Program (Grant No. 2011GB108004), and by the National Natural Science Foundation of China (Grant Nos. 11075177, 91026002, 91126002, 11175203, 51101152).

References

[1] I. Smid, H.D. Pacher, G. Vieider, U. Mszanowski, Y. Igitkhanov, G. Janeschitz, J. Schlosser, L. Plochl, J. Nucl. Mater. 233–237 (1996) 701–707.
[2] T. Hino, M. Akiba, Fusion Eng. Des. 49–50 (2000) 97–105.
[3] P. Norajitra, L.V. Boccaccini, E. Diegele, V. Filatov, A. Gervash, R. Giniyatulin, S. Gordeev, V. Heinzel, G. Janeschitz, J. Konys, W. Krauss, R. Kruessmann, S. Malang, I. Mazul, A. Moeslang, C. Petersen, G. Reimann, M. Rieth, G. Rizzi, M. Rumyantsev, R. Ruprecht, V. Slobodtchouk, J. Nucl. Mater. 329–333 (2004) 1594–1598.
[4] E. Diegele, R. Krussmann, S. Malang, P. Norajitra, G. Rizzi, Fusion Eng. Des. 66–68 (2003) 383–387.
[5] P. Norajitra, L.V. Boccaccini, A. Gervash, R. Giniyatulin, N. Holstein, T. Ihli, G. Janeschitz, W. Krauss, R. Kruessmann, V. Kuznetsov, A. Makhankov, I. Mazul, A. Moeslang, I. Ovchinnikov, M. Rieth, B. Zeep, J. Nucl. Mater. 367–370 (2007) 1416–1421.
[6] H. Kurishita, S. Kobayashi, K. Nakai, T. Ogawa, A. Hasegawa, K. Abe, H. Arakawa, S. Matsuo, T. Takida, K. Takebe, M. Kawai, N. Yoshida, J. Nucl. Mater. 377 (2008) 34–40.
[7] H. Kurishita, Y. Amano, S. Kobayashi, K. Nakai, H. Arakawa, Y. Hiraoka, T. Takida, K. Takebe, H. Matsui, J. Nucl. Mater. 367–370 (2007) 1453.
[8] Y. Zhang, A.V. Ganeev, J.T. Wang, J.Q. Liu, I.V. Alexandrov, Mater. Sci. Eng., A 503 (2009) 37–40.
[9] Y. Ishijima, H. Kurishita, K. Yubuta, H. Arakawa, M. Hasegawa, Y. Hiraoka, T. Takida, K. Takebe, J. Nucl. Mater. 329–333 (2004) 775–779.
[10] H. Kurishita, T. Kuwabara, M. Hasegawa, S. Kobayashi, K. Nakai, J. Nucl. Mater. 343 (2005) 318–324.
[11] N. Nita, R. Schaeublin, M. Victoria, J. Nucl. Mater. 329–333 (2004) 953–957.
[12] M. Samaras, P.M. Derlet, H.V. Swygenhoven, M. Victoria, Phys. Rev. Lett. 88 (2002) 12.
[13] Y. Kim, K.H. Lee, E.-P. Kim, D.-I. Cheong, S.H. Hong, Int. J. Refract. Met. Hard Mater. 27 (2009) 842–846.
[14] M. Rieth, B. Dafferner, J. Nucl. Mater. 342 (2005) 20–25.
[15] M.A. Yar, S. Wahlberg, H. Bergqvist, H.G. Salem, M. Johnsson, M. Muhammeda, J. Nucl. Mater. 408 (2011) 129–135.
[16] A. Muñoz, M.A. Monge, B. Savoini, M.E. Rabanal, G. Garces, R. Pareja, J. Nucl. Mater. 417 (2011) 508–511.
[17] M.A. Yar, S. Wahlberg, H. Bergqvist, H.G. Salem, M. Johnsson, M. Muhammeda, J. Nucl. Mater. 412 (2011) 227–232.
[18] I. Wesemann, W. Spielmann, P. Heel, A. Hoffmann, Int. J. Refract. Met. Hard Mater. 28 (2010) 687–691.
[19] Y. Kim, M.-H. Hong, S.H. Lee, E.-P. Kim, S. Lee, J.-W. Noh, Met. Mater. Int. 12 (3) (2006) 245–248.
[20] M.V. Aguirre, A. Martín, J.Y. Pastor, Metall. Mater. Trans. A 40 (2009) 2283–2290.
[21] M.V. Aguirre, A. Martín, J.Y. Pastor, J. Nucl. Mater. 404 (2010) 203–209.
[22] S.I. Cha, S.H. Hong, Mater. Sci. Eng., A 356 (2003) 381–389.
[23] R. Roy, D. Agrawal, J. Cheng, S. Gedevanishvili, Nature 399 (1999) 668–670.
[24] K. Saitou, Scripta Mater. 54 (2006) 875–879.
[25] J. Cheng, D. Agrawal, Y. Zhang, R. Roy, Mater. Lett. 56 (2002) 587–592.
[26] S. Wurster, R. Pippan, Scripta Mater. 60 (2009) 1083–1087.
[27] G. Prabhu, A. Chakraborty, B. Sarma, Int. J. Refract. Met. Hard Mater. 27 (2009) 545–548.
[28] I. Barin, Thermochemical Data of Pure Substances, third ed., Wiley-VCH, Verlag, GmbH, Weinheim, 1995.
[29] K. Wang, X.P. Wang, R. Liu, T. Hao, T. Zhang, C.S. Liu, Q.F. Fang, J. Nucl. Mater. (2011), http://dx.doi.org/10.1016/j.jnucmat.2011.11.012.
[30] R. Liu, T. Hao, K. Wang, T. Zhang, X.P. Wang, C.S. Liu, Q.F. Fang, J. Nucl. Mater. (2011), http://dx.doi.org/10.1016/j.jnucmat.2011.11.013.
[31] ITER, ITER Materials Properties Handbook ITER Document No. G 74 MA 9 00-11-10 W 0.1, 2001.